Electronic Supplementary Material (ESI) for Journal of Materials Chemistry A.

Supplementary Information

Li-ion conductivity in $Li_2OHCl_{1-x}Br_x$ solid electrolytes: grains, grain boundaries and interfaces

Hyeon Jeong Lee[a], Brigita Darminto[a], Sudarshan Narayanan[a], Maria Diaz-Lopez[b], Albert W. Xiao[a], Yvonne Chart[a], Ji Hoon Lee[c], James A. Dawson[d,e], and Mauro Pasta[a,*]

[a]Department of Materials, University of Oxford, Parks Road, Oxford OX1 3PH, United Kingdom
[b]Diamond Light Source Ltd., Diamond House, Harwell Science and Innovation Campus, Didcot, OX11 0DE, United Kingdom
[c]School of Materials Science and Engineering, Kyungpook National University, 80 Daehak-ro, Buk-gu, Daegu 41566, Republic of Korea
[d]Chemistry - School of Natural and Environmental Sciences, Newcastle University, Newcastle upon Tyne, NE1 7RU, United Kingdom
[e]Centre for Energy, Newcastle University, Newcastle upon Tyne, NE1 7RU, United Kingdom

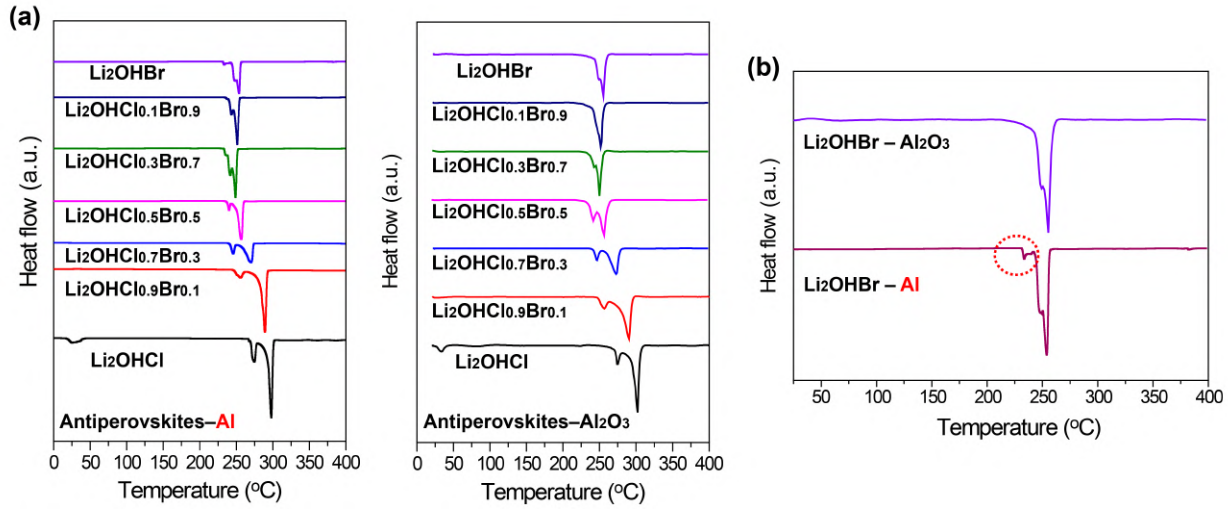

Fig. S1 (a) DSC spectra of $Li_2OHCl_{1-x}Br_x$ (x=0, 0.1, 0.3, 0.5, 0.7, 0.9, 1) antiperovskites measured with aluminium pan(left) and alumina crucible(right). A small endothermic peak was observed below the local disordering temperature of the $Li_2OHCl_{1-x}Br_x$ series which was measured in an aluminium pan and lid setup. (b) Comparative DSC spectra of Li_2OHBr measured with alumina crucible and aluminium pan.

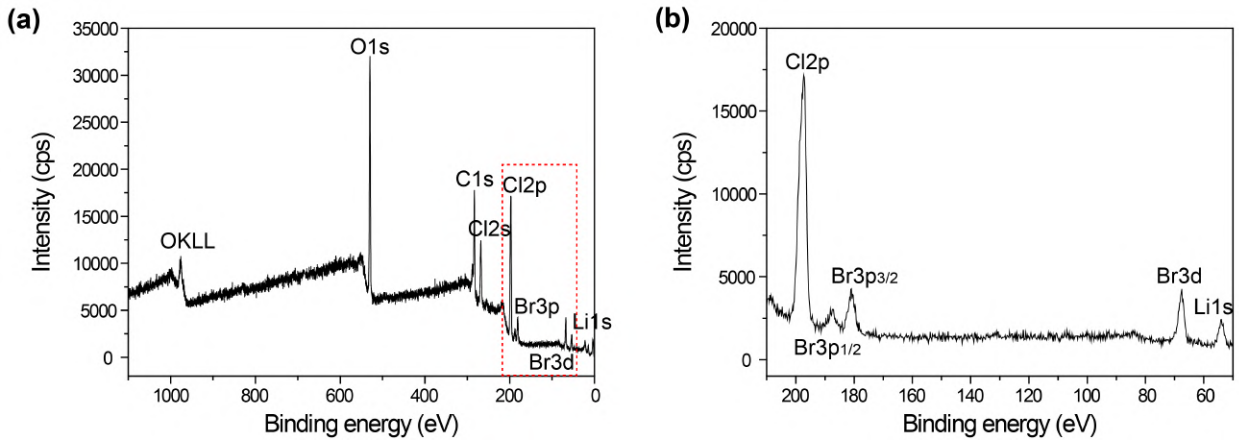

Fig. S2 (a) Survey spectrum of as-synthesized $Li_2OHCl_{0.9}Br_{0.1}$. (b) A zoomed survey spectrum in the energy range of 50–210 eV. Al 2p (∼75 eV) and Al 2s (∼120 eV) peaks were not observed.

	Li_2OHCl			Li_2OHBr
	phase a	phase b	LiCl	phase a
Space group	$Pmc2_1$	$Pm\bar{3}m$	$Fm\bar{3}m$	$Pm\bar{3}m$
Lattice parameter (Å)	a=3.8777(2) b=3.8301(2) c=8.0004(4)	a=3.9080(1)	a=5.1478(8)	a=4.04727(3)
Volume ($Å^3$)	118.822(8)	59.684(5)	136.42(6)	66.296(2)
Weight fraction (%)	52.8(1)	43.4(5)	3.7(2)	100
R_p(%)	8.81			5.17
R_{wp}(%)	12.15			7.14
R_{exp}(%)	1.25			0.96

Table S1. Refined lattice parameters, cell volumes, and weight fraction of each phase in Li_2OHCl and Li_2OHBr.

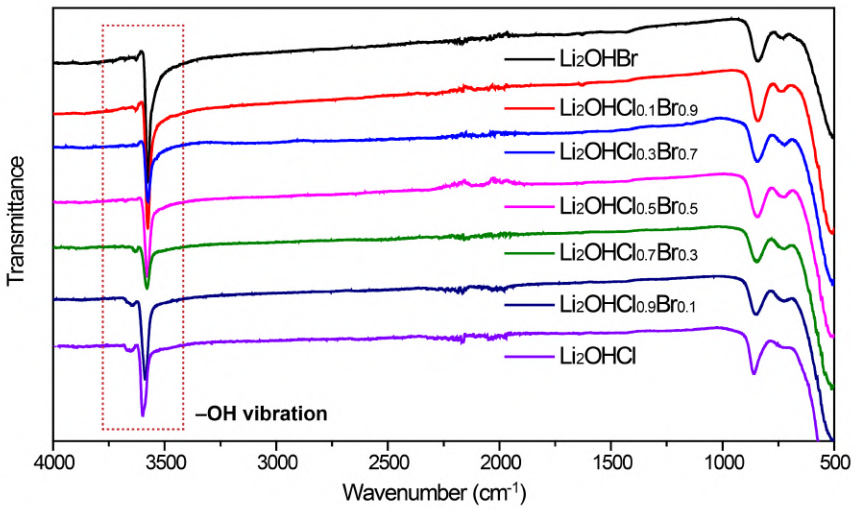

Fig. S3 FT-IR spectra of $Li_2OHCl_{1-x}Br_x$ (x=0, 0.1, 0.3, 0.5, 0.7, 0.9, 1) antiperovskites.

Composition	**Lattice parameter(Å)**
$Li_2OHCl_{0.9}Br_{0.1}$	3.92104
$Li_2OHCl_{0.7}Br_{0.3}$	3.95091
$Li_2OHCl_{0.5}Br_{0.5}$	3.97906
$Li_2OHCl_{0.3}Br_{0.7}$	4.00665
$Li_2OHCl_{0.1}Br_{0.9}$	4.03444
Li_2OHBr	4.04727

Table S2. Lattice parameters of cubic phase $Li_2OHCl_{1-x}Br_x$ based on XRD patterns measured at the room temperature.

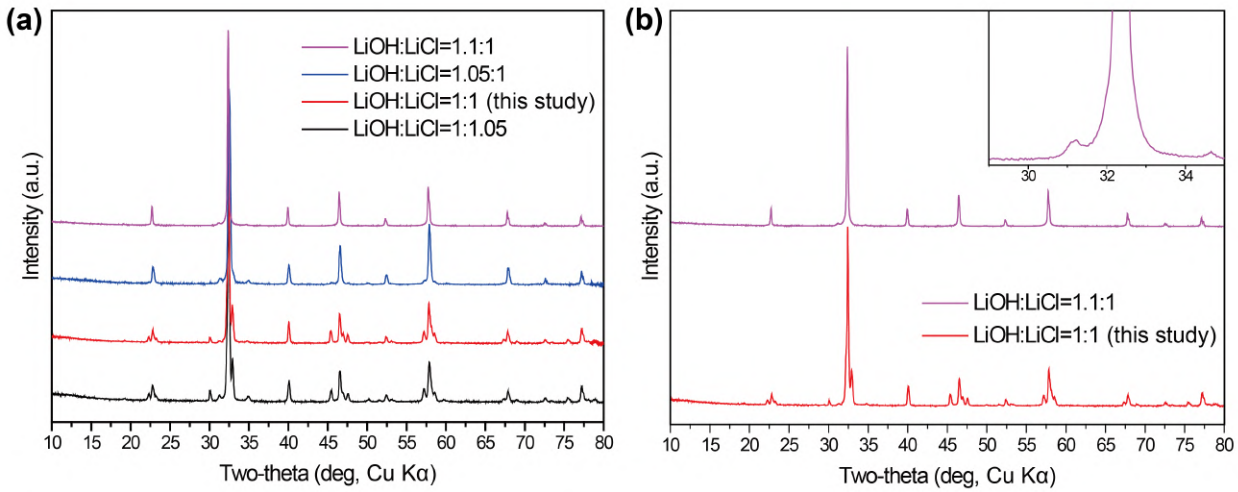

Fig. S4 Comparison of XRD patterns for lithium hydroxide chlorides synthesized with varied LiOH/LiCl molar ratios. Sub-stoichiometric lithium hydroxide chlorides were synthesized under LiCl deficiency (Molar ratios of 1.05:1 (as LiOH:LiCl) and 1.1:1 were used.). The phase transformation in sub-stoichiometric lithium hydroxide chlorides was observed and they contain minor impurities as well.

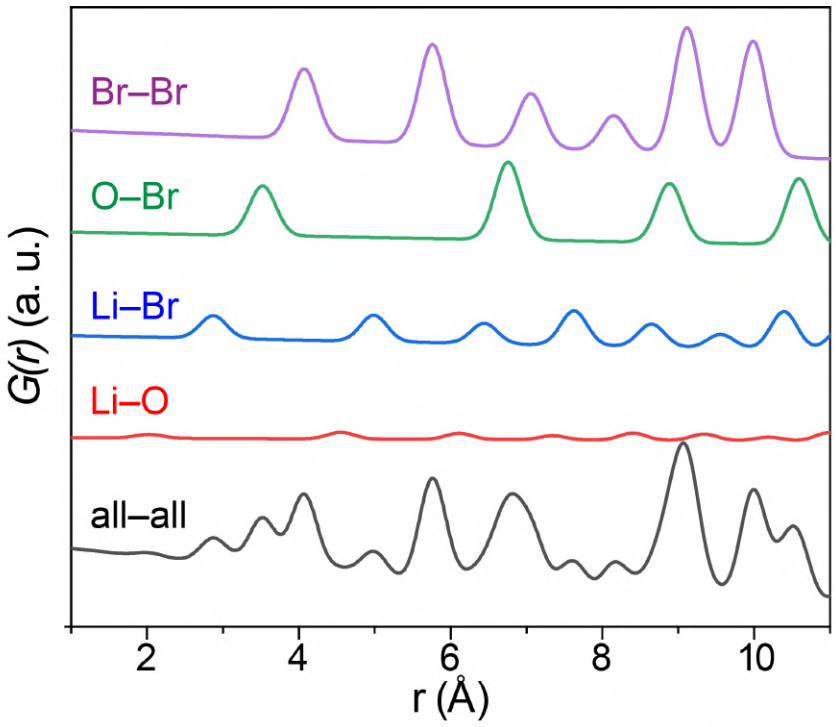

Fig. S5 Calculated PDF pattern of Li_2OHBr with the $Pm\bar{3}m$ symmetry, and their partial PDFs of different atom-atom pairs.

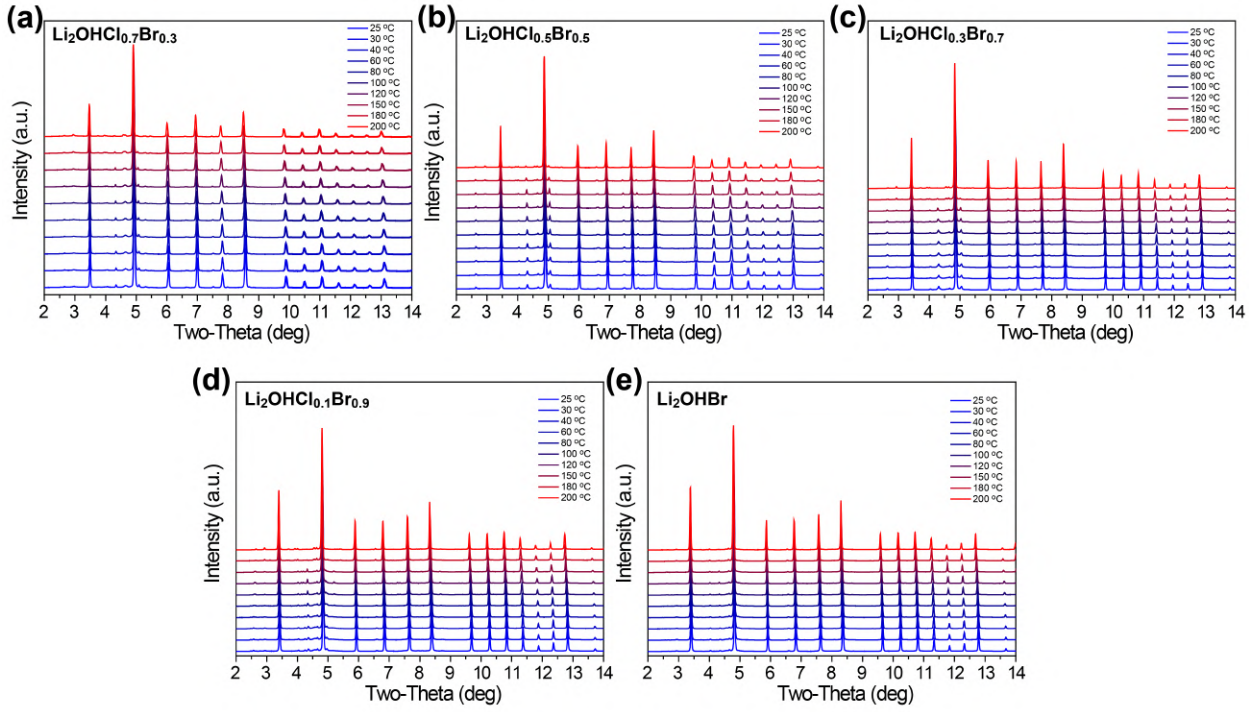

Fig. S6 *In situ* high temperature XRD patterns of (a) $Li_2OHCl_{0.7}Br_{0.3}$, (b) $Li_2OHCl_{0.5}Br_{0.5}$, (c)$Li_2OHCl_{0.3}Br_{0.7}$, (d) $Li_2OHCl_{0.1}Br_{0.9}$, and (e) Li_2OHBr during heating process in the temperature range of 25–200 °C.

Temperature (°C)	Li_2OHCl	$Li_2OHCl_{0.9}Br_{0.1}$	$Li_2OHCl_{0.7}Br_{0.3}$	$Li_2OHCl_{0.5}Br_{0.5}$	$Li_2OHCl_{0.3}Br_{0.7}$	$Li_2OHCl_{0.1}Br_{0.9}$	Li_2OHBr
25		3.92104	3.95091	3.97906	4.00665	4.03444	4.0472
30		3.9217	3.95164	3.98002	4.00737	4.03518	4.04795
40	3.91077	3.92314	3.95317	3.98137	4.00895	4.03676	4.04956
60	3.91371	3.92608	3.95634	3.98466	4.0122	4.04008	4.05285
80	3.91685	3.92916	3.95971	3.988	4.01568	4.04367	4.05643
100	3.92002	3.93234	3.96322	3.9917	4.01934	4.04743	4.06018
120	3.92371	3.93555	3.96683	3.99588	4.02317	4.05131	4.06404
150	3.92807	3.94029	3.97241	4.00127	4.02887	4.05705	4.06978
180	3.93269	3.94519	3.97813	4.00718	4.03481	4.06304	4.076016
200	3.93623	3.94873	3.98212	4.0116	4.03911	4.06742	4.080355

Table S3. Lattice parameters of $Li_2OHCl_{1-x}Br_x$ (x=0, 0.1, 0.3, 0.5, 0.7, 0.9, 1) antiperovskites under the cubic symmetry measured at the temperature range of 25–200 °C

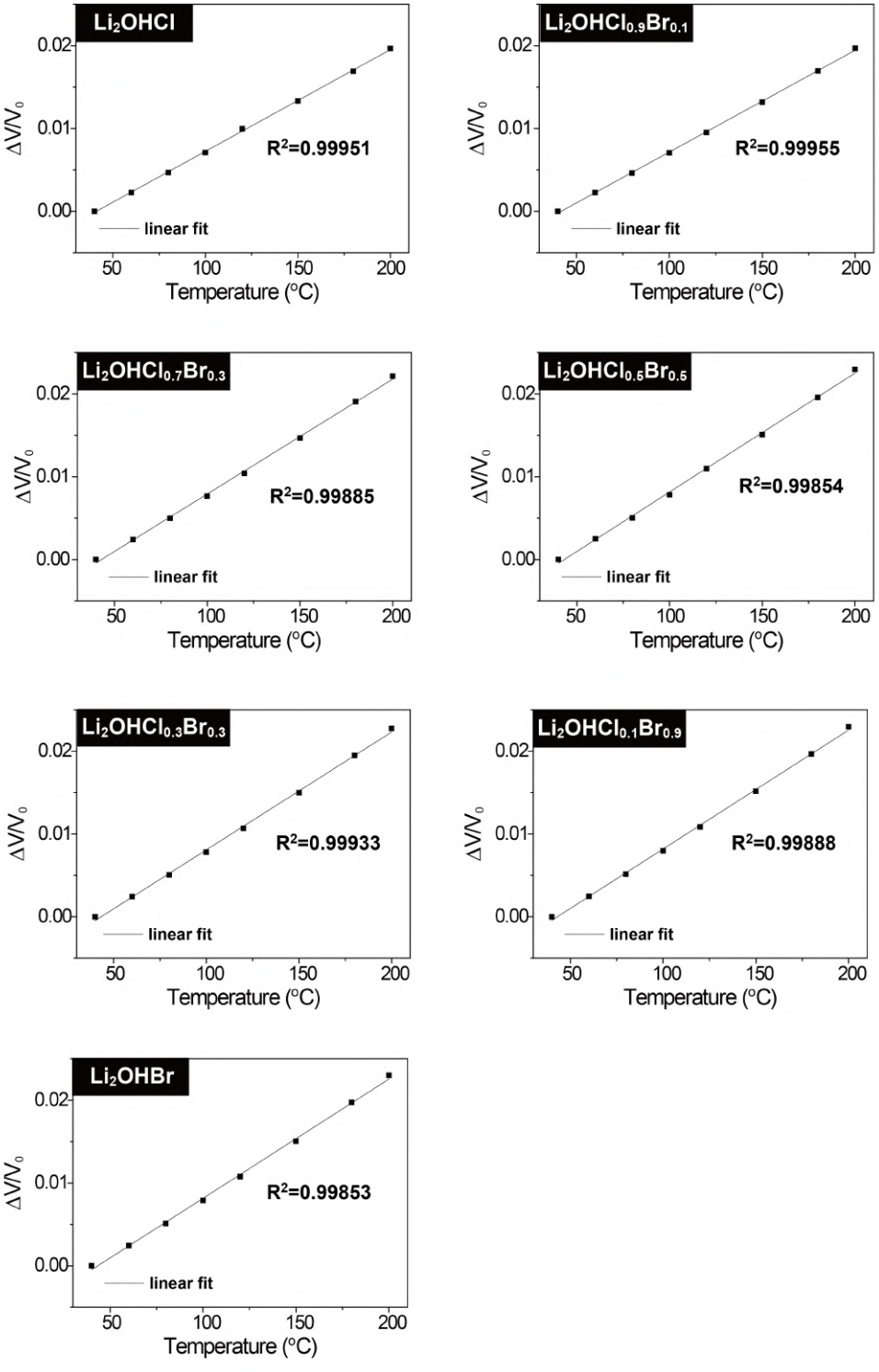

Fig. S7 Volumetric thermal expansion curves of $Li_2OHCl_{1-x}Br_x$.

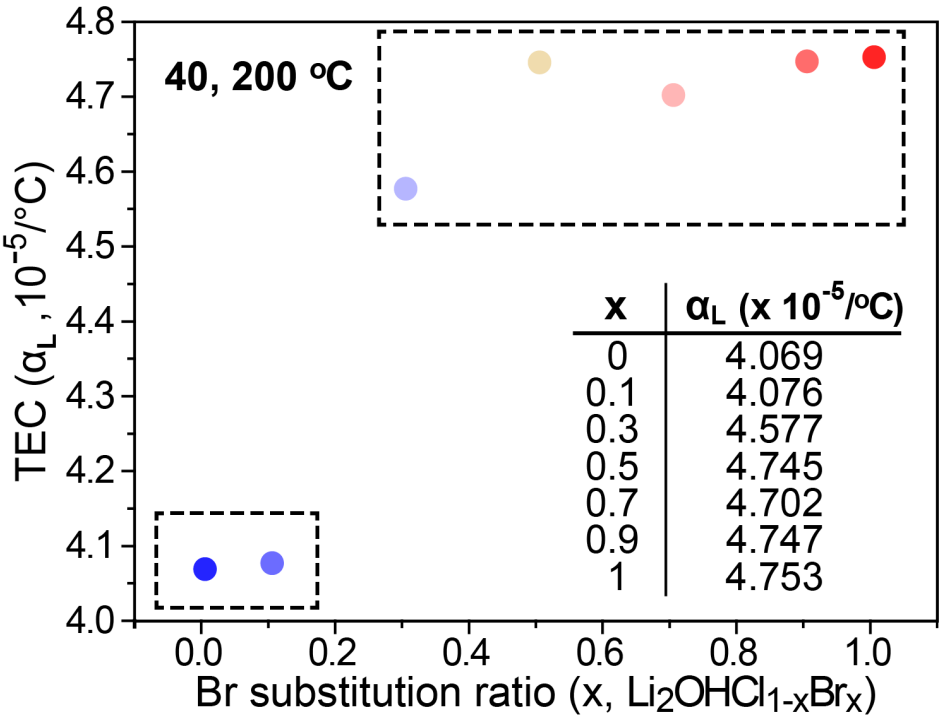

Fig. S8 Linear thermal expansion coefficients (α_L) calculated based on the lattice parameters at 40 and 200 °C

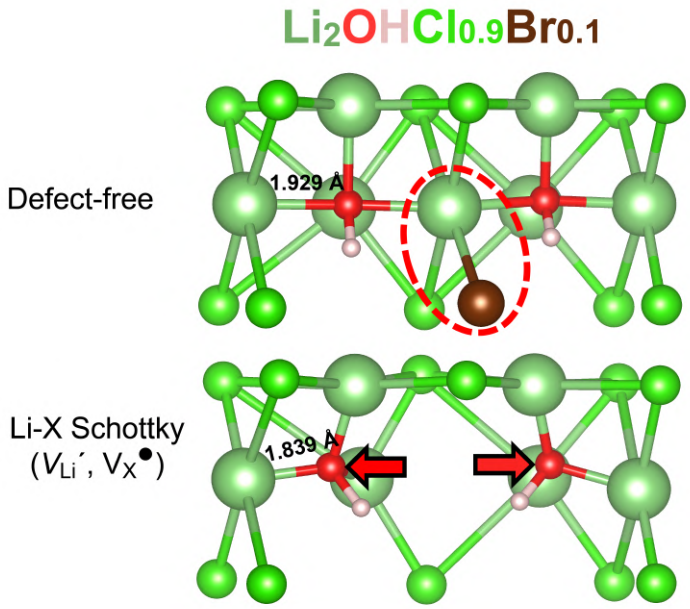

Fig. S9 Schematic illustration of the local structural relaxation resulting from the introduction of a Li-X Schottky defect pair in $Li_2OHCl_{0.9}Br_{0.1}$.

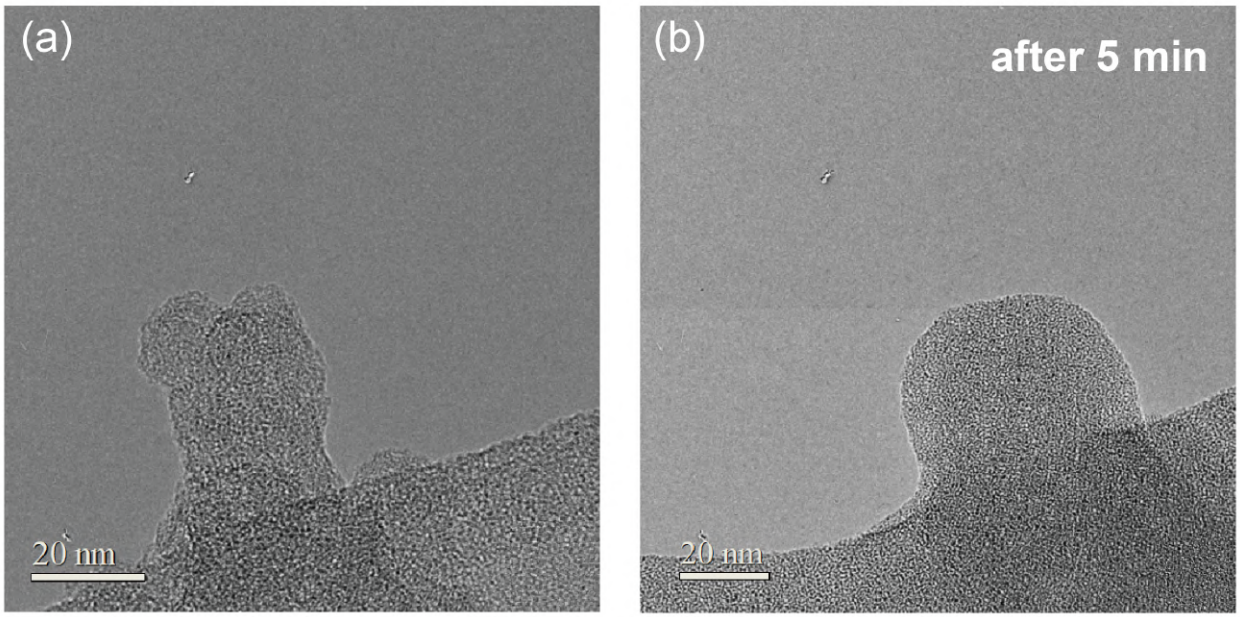

Fig. S10 TEM images of $Li_2OHCl_{0.9}Br_{0.1}$ before (a) and after (b) 5 min of exposure in the same region. Particles had agglomerated and transformed to a fully amorphous state.

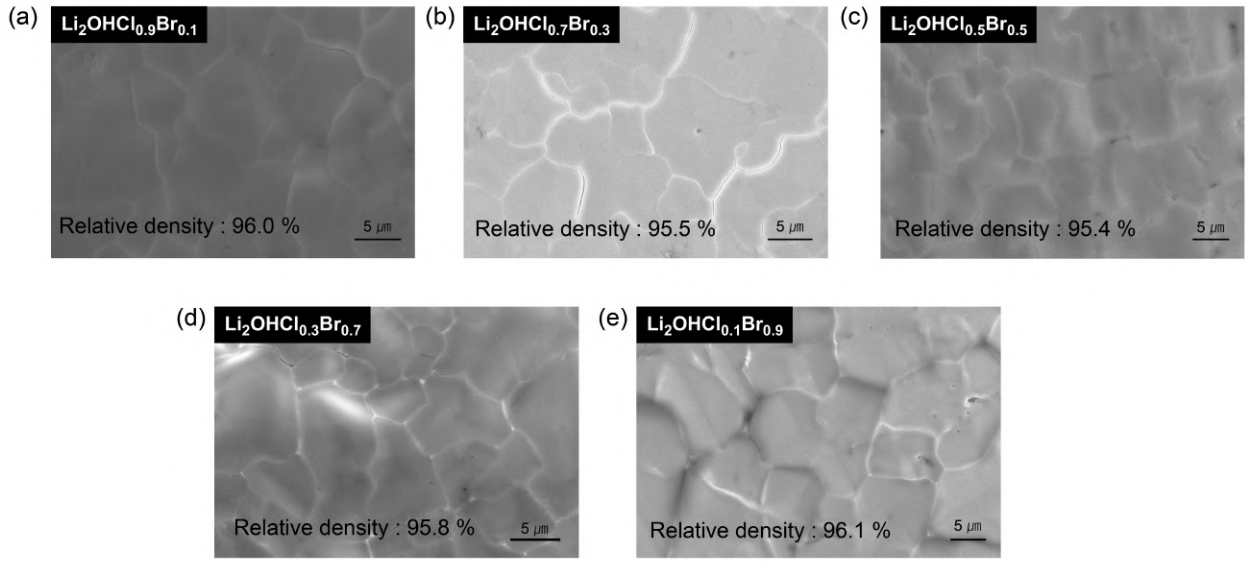

Fig. S11 Cross-sectional SEM images and relative densities of $Li_2OHCl_{1-x}Br_x$ pellets ((a–e), x=0.1, 0.3, 0.5, 0.7, and 0.9, respectively).

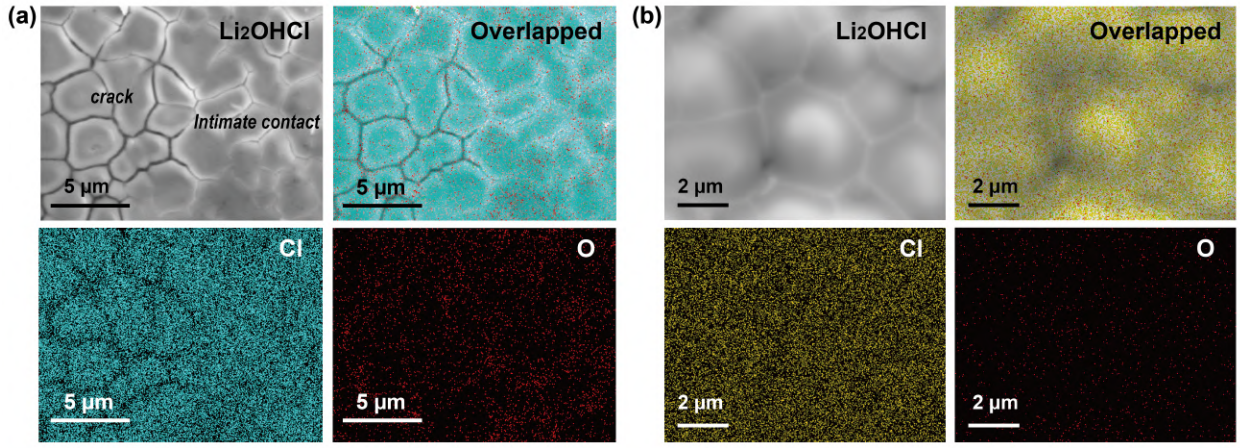

Fig. S12 Cross-sectional SEM images of Li_2OHCl pellet and corresponding mappings with respect to Cl and O with(a) and without(b) polishing.

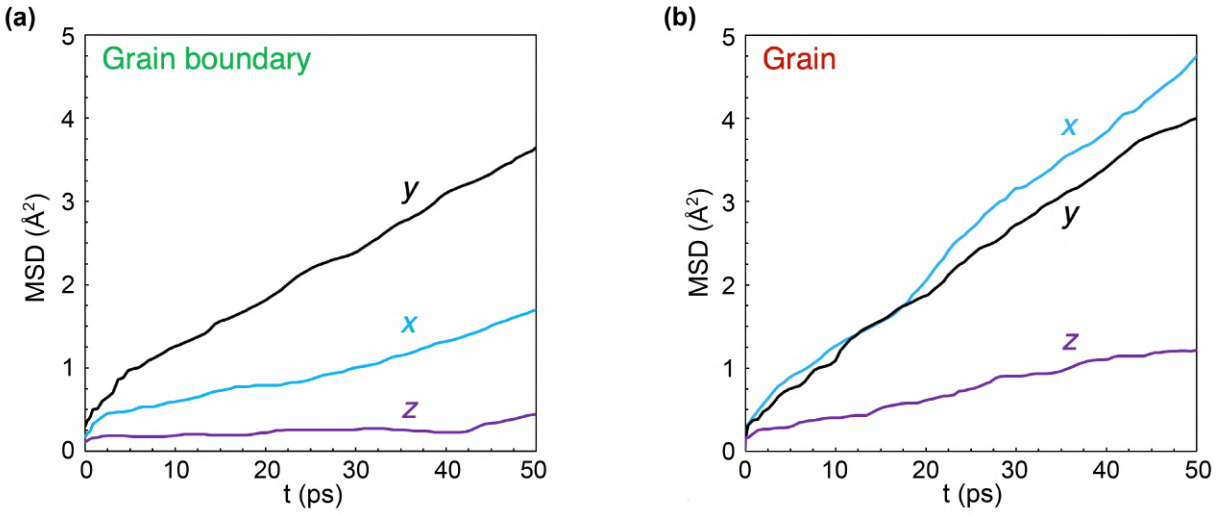

Fig. S13 MSDs of Li ions for the grain boundary (a) and grain components (b) of the Li_2OHBr Σ3(111) grain boundary at 1000 K in the x, y and z directions.

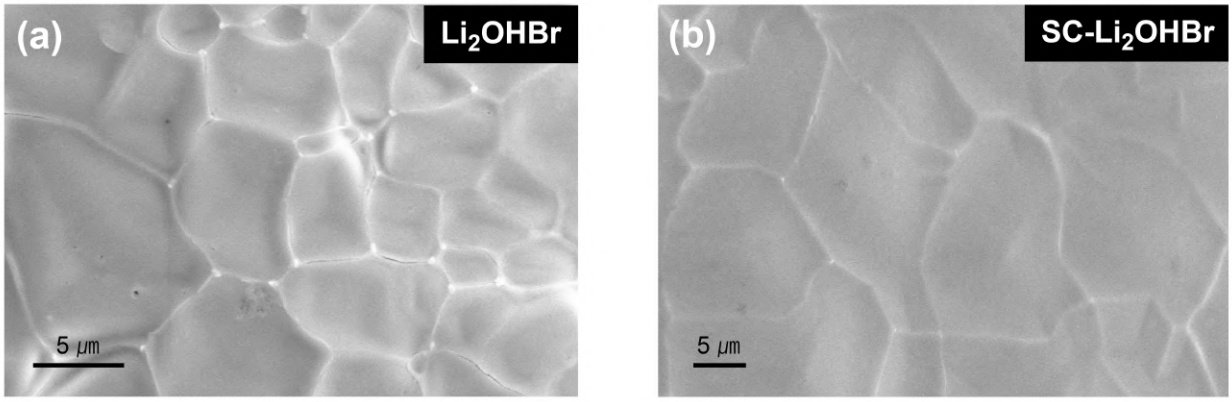

Fig. S14 Cross-sectional SEM images of (a) Li_2OHBr and (b) slow-cooled Li_2OHBr pellets based on the melting and solidification process.

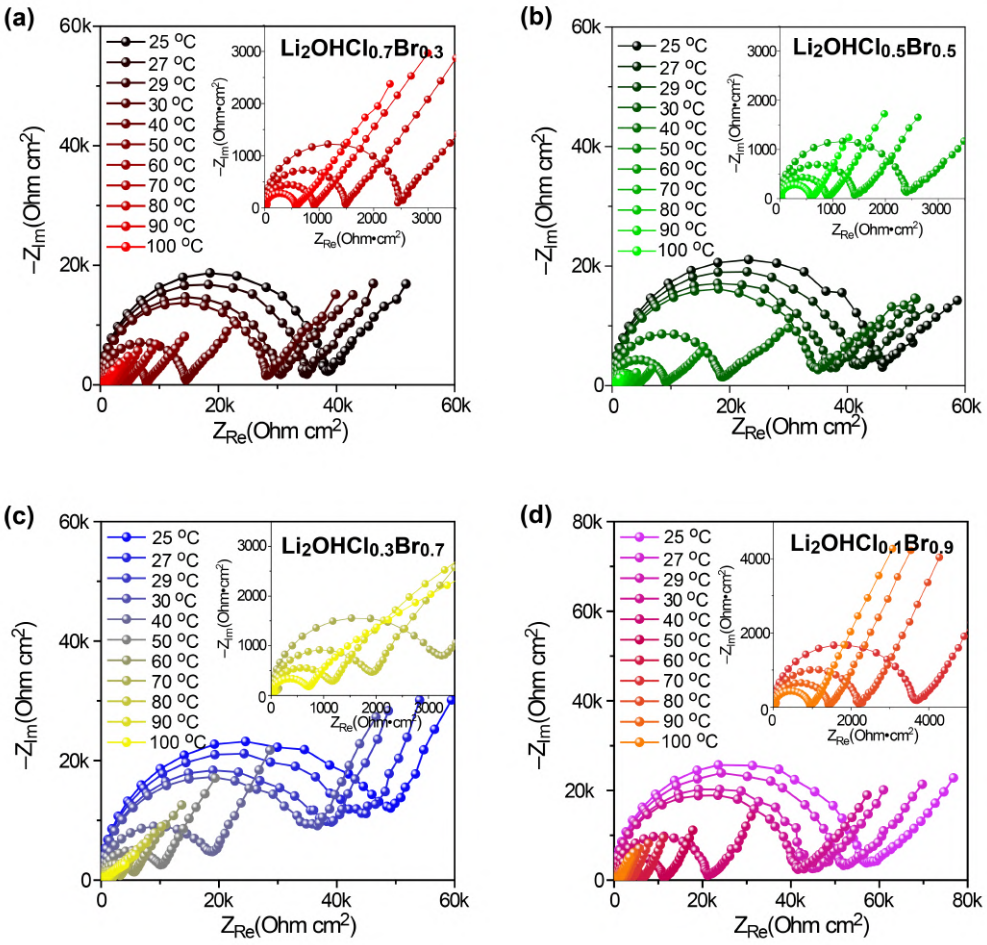

Fig. S15 EIS spectra of (a) $Li_2OHCl_{0.7}Br_{0.3}$, (b) $Li_2OHCl_{0.5}Br_{0.5}$, (c) $Li_2OHCl_{0.3}Br_{0.7}$, and (d) $Li_2OHCl_{0.1}Br_{0.9}$ measured at 25–100 °C under Ni/Ni symmetric configuration.

	Li_2OHCl	$Li_2OHCl_{0.9}Br_{0.1}$	$Li_2OHCl_{0.7}Br_{0.3}$	$Li_2OHCl_{0.5}Br_{0.5}$	$Li_2OHCl_{0.3}Br_{0.7}$	$Li_2OHCl_{0.1}Br_{0.9}$	Li_2OHBr
25 °C	0.001927	0.00252	0.001799	0.001537	0.00145	0.00124	0.001291
27 °C	0.002239	0.002837	0.001973	0.001695	0.001599	0.001364	0.001425
29 °C	0.002886	0.003229	0.002262	0.001842	0.001858	0.001561	0.001608
30 °C	0.003175	0.003346	0.002447	0.002018	0.001979	0.001684	0.001728
40 °C	0.005913	0.0062	0.00474	0.003749	0.003753	0.003265	0.003365
50 °C	0.010696	0.011272	0.008714	0.00763	0.007539	0.006176	0.006431
60 °C	0.017782	0.019559	0.015719	0.016804	0.011991	0.011069	0.011967
70 °C	0.030866	0.032089	0.027457	0.029142	0.020399	0.019312	0.020973
80 °C	0.047476	0.051119	0.046709	0.049309	0.034139	0.032756	0.035138
90 °C	0.072773	0.078135	0.077201	0.07818	0.061679	0.049463	0.055141
100 °C	0.119495	0.115481	0.122353	0.119882	0.106041	0.07506	0.084045
Activation energy (eV)	0.5288	0.5243	0.5740	0.6060	0.5703	0.5645	0.5747

Table S4. Li-ion conductivities of $Li_2OHCl_{1-x}Br_x$ (x=0, 0.1, 0.3, 0.5, 0.7, 0.9, 1) antiperovskites measured at various temperatures and the resultant activation energies.

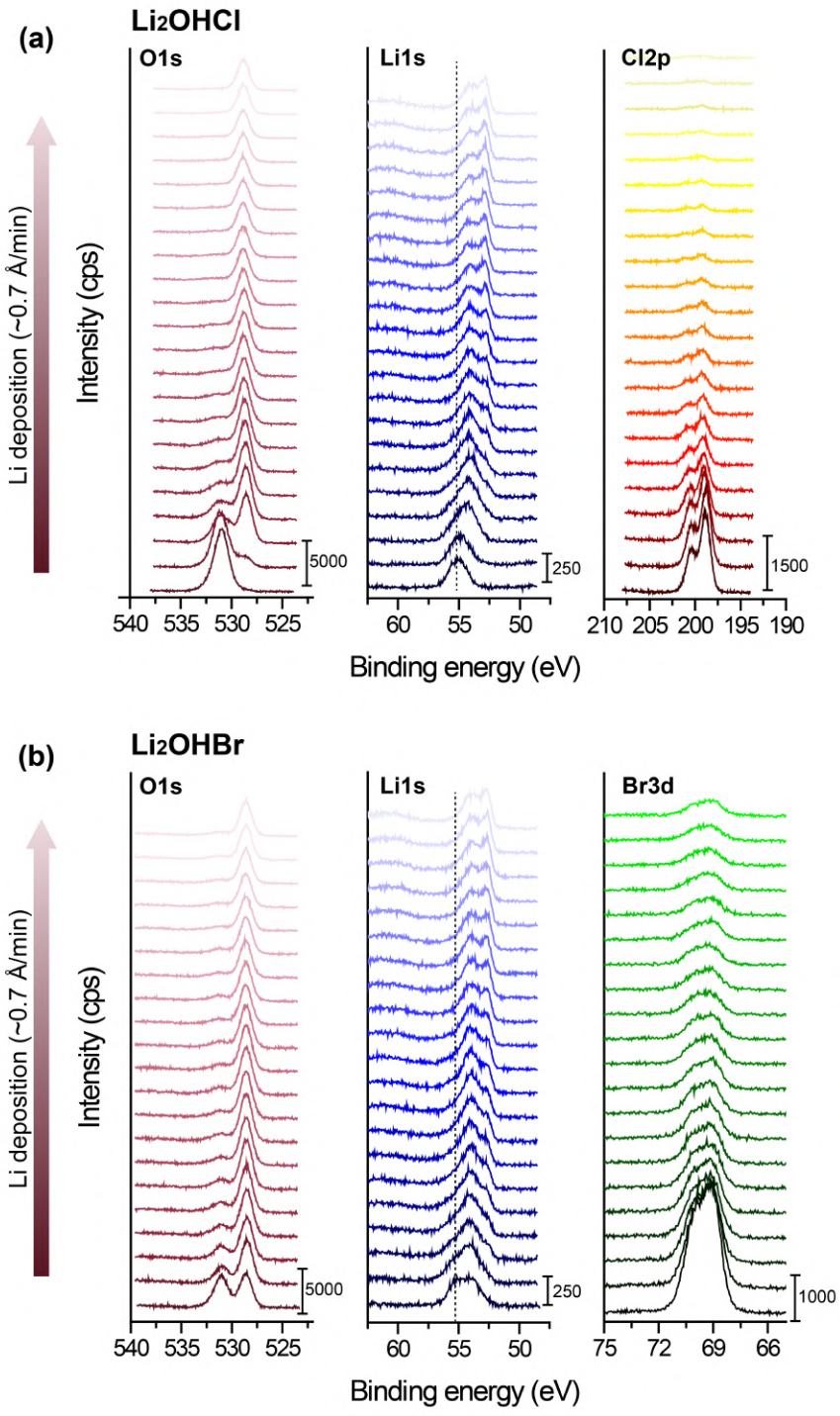

Fig. S16 O 1s, Li 1s, Cl 2p, and Br 3d XPS spectra of Li_2OHCl (a) and Li_2OHBr (b) as a function of increasing amount of lithium metal being deposited (from bottom to top) at room temperature.

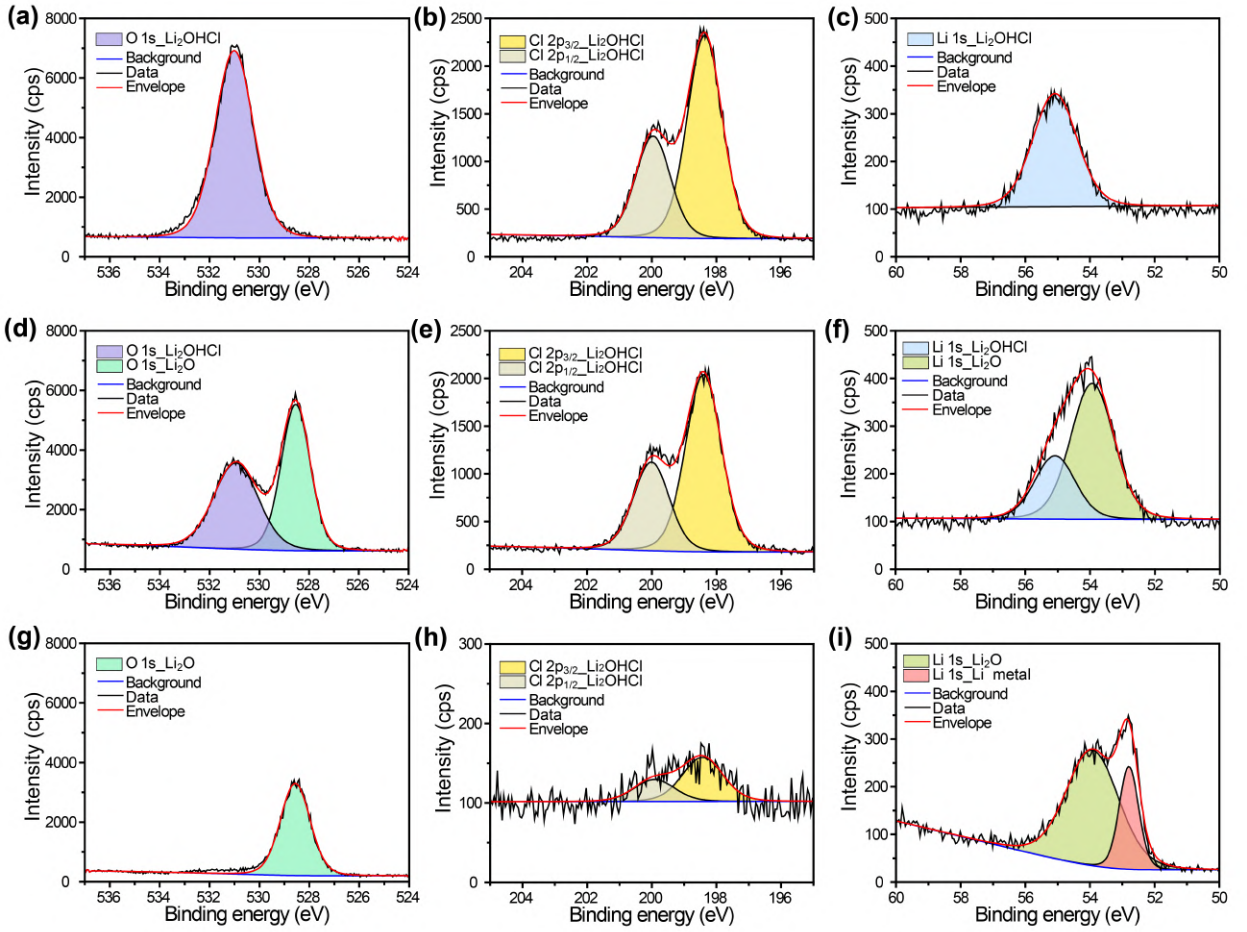

Fig. S17 Deconvoluted O1s (a, d and g), Cl2p (b, e, and h), and Li1s (c, f, and i) XPS spectra of Li_2OHCl before (a–c), during Li metal sputtering with the estimated Li-metal thickness of 3.5 Å (d–f) and 12.6 nm (g–i).

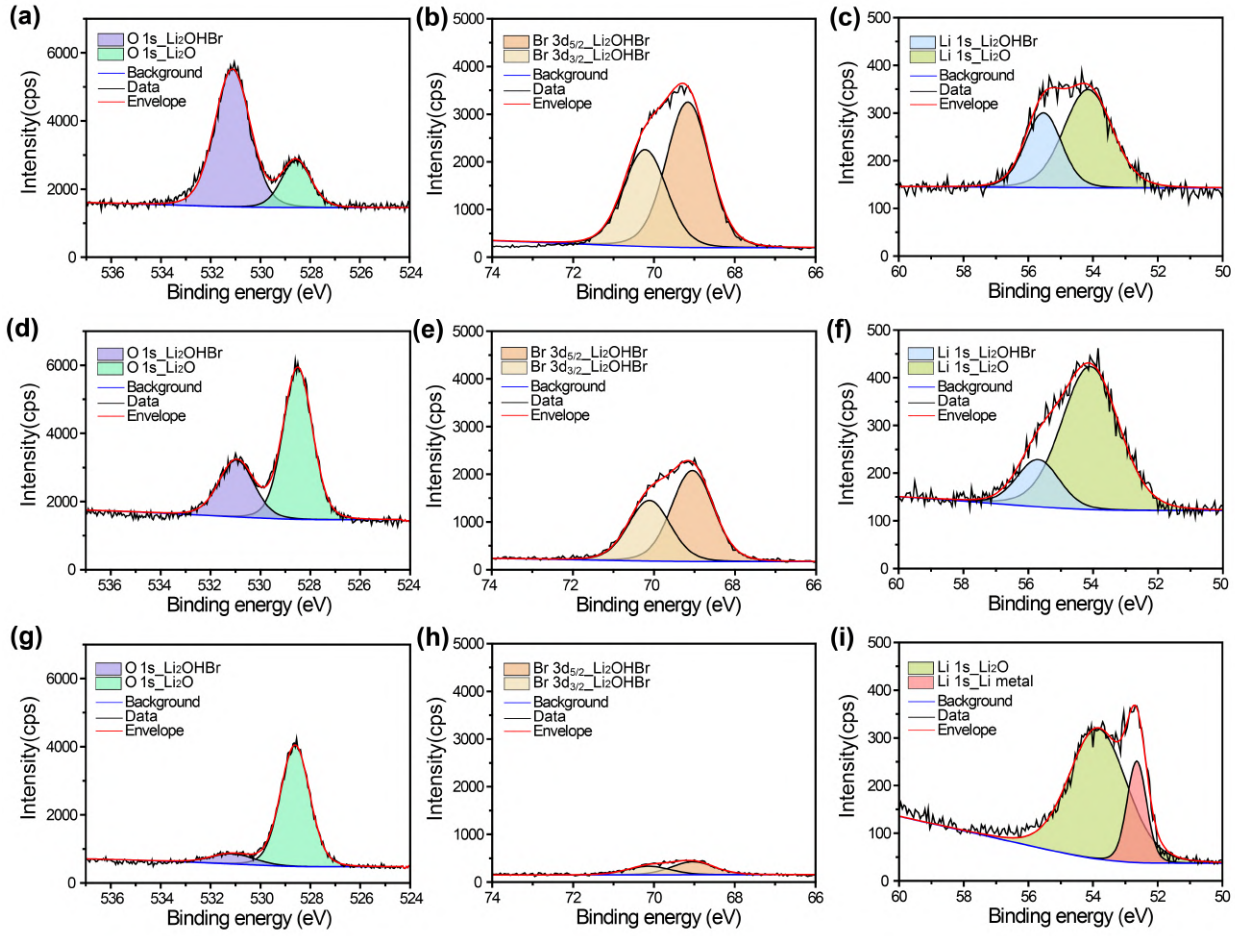

Fig. S18 Deconvoluted O1s (a, d and g), Br3d (b, e, and h), and Li1s (c, f, and i) XPS spectra of Li_2OHBr during Li metal sputtering with the estimated Li-metal thickness of 3.5 Å (a–c), 10.5 Å (d–f) and 14 nm (g–i).